Proceedings of the 2nd Marine Energy Technology Symposium
METS2014
April 15-18, 2014, Seattle, WA

HYDROKINETIC TURBINES AT HIGH BLOCKAGE RATIO

Arshiya Hoseyni-Chime
Mechanical Engineering Department
University of Washington
Seattle, WA, 98195

Philip C. Malte
Mechanical Engineering Department
University of Washington
Seattle, WA, 98195

[1]Corresponding author: ahc9@uw.edu

1 ABSTRACT

This study investigates the possibility of using hydrokinetic turbines for both power generation and flow control, with the potential to replace some of the sluice gates in constructed channels. Theoretical and numerical approaches are used to model the horizontal axis hydrokinetic turbines (HAHTs) in open channel flows where blockage ratio is high.

The theoretical method uses one-dimensional control volume analysis to predict maximum power that an ideal rotor can extract from the flow as a function of the axial induction factor and the blockage ratio. This method is then compared to the three-dimensional actuator disc model (ADM) developed in the commercial computational fluid dynamic (CFD) code ANSYS Fluent 14.0. This model uses a porous media to represent the HAHTs and Reynolds-Average Navier-Stokes (RANS) equations along with the volume of fluid (VoF) model to solve for the flow field and track the free surface of the water. Finally, the HAHTs are modeled with a more advanced approach, this being the virtual blade model (VBM) in Fluent, which uses blade element theory to consider geometry of the blade. The effects of tip-speed-ratio (TSR) and pitch angle on turbine power extraction and total flow power loss are computed.

At high blockage ratios, due to large changes in free surface elevation, surface must be tracked using the VoF model. The VBM is thought to be the best representation of the HAHT at high blockage ratios compared to 1D theory and ADM. Both one-dimension theory and ADM overpredicted the extracted power from the turbines by about 43 percent compared to the VBM. In addition, 1D theory underpredicted the extracted power from the total flow by 30 percent relative to the VBM; while this difference was about 10 percent with the ADM.

2 INTRODUCTION

Large constructed waterways are found worldwide, frequently used for irrigation of agricultural land. Typically, flow control on these canals is accomplished by sluice gates and drops, with power generation sometimes obtained by relatively low head turbines placed at drops. Flow power loss at a sluice gate placed at one location on a large canal of 100-200 m^3/s flow rate can be about 1 MW. Given that this dissipated power is wasted, it is desirable to capture some of this loss in terms of useful power. Horizontal axis hydrokinetic turbines (HAHTs) are possible candidates for replacing traditional gates to not only control the flow, but also to generate power. Three methods are used in this paper to represent HAHTs in a flow with high blockage, including one-dimensional linear momentum theory, actuator disc model (ADM), and virtual blade model (VBM).

The one-dimensional theory predicts the maximum useful power that can be extracted from the flow using conservation laws. Lanchester-Betz found that an ideal rotor is able to extract up to 59% of the incoming kinetic power of the flow using streamtube analysis [1]. This analysis was then applied to the turbines in constrained channels by Garrett et al. [2] to find that a turbine's efficiency can exceed the Lanchester-Betz limit by a factor of $(1 - BR)^{-2}$ when flow is constrained. Blockage ratio, BR, is defined as the cross-sectional area of the turbines over the cross-sectional area of the channel. This one-dimensional theory is only valid for small Froude number, BR and surface deflection due to power extraction behind the turbines is neglected. Froude number, Fr, is the ratio of inertia to gravity forces. Whelan et al. [3] improved this

analysis by including the free surface drop behind the turbines. It was found that at high BRs, a subcritical and a supercritical solution exist. Also, power coefficient of the turbines depended on the bypass flow velocity, velocity through the turbines, and the velocity at the end of the expansion region normalized by the incoming flow velocity. Polagye [4] extended the theory to find the power loss due to wake mixing downstream of the turbines. This one-dimensional theory is used to find an upper limit for useful power extraction by the turbines and to estimate the dissipated power due to wake mixing.

Another method commonly used in literature to predict performance of HAHTs is Reynolds-Averaged Navier-Stokes (RANS) equations along with actuator disc model (ADM) [5], [6], [7], [8], [9], [10]. This method approximates the forces that a turbine applies to the flow over a disc with the same diameter. MacLeod et al. [5] used a slip condition (rigid lid) to treat the free surface. It was found that increasing ambient turbulence intensity results in faster wake recovery. Sun et al. [6], [7] used the volume of fluid (VoF) method to track the free surface. As Froude number was increased, higher surface drop was observed behind the turbine, more power was extracted from the flow, and wake recovered slower. Harrison et al. [8] used RANS-ADM simulations for modeling flow behind turbines and compared them to experimental data measured behind porous discs. Velocities and turbulence intensities were well matched in the far wake region. Nishino et al. [9] used 3D RANS-ADM with a rigid lid free surface boundary condition to investigate the effects of channel geometry and blockage on performance of turbines. It was found that the aspect ratio of the channel had a negligible effect on the power coefficient; however, as blockage ratio was increased, a significantly higher power coefficient was achieved.

Whelan et al. [3] used the blade element model (BEM) in a 1D code to predict the power coefficient and thrust coefficient of a tidal turbine at both zero blockage and high blockage ratios. Comparison to experimental data showed good agreement at low TSRs. This is in agreement with the findings of Batten et al. [10], which used RANS-BEM to predict the performance of a turbine at low blockage without tracking the free surface. Consul et al. [11] explored the effects of blockage ratio and free stream deformation on the performance of a cross-flow turbine using 2D RANS simulations. At low blockage, the power coefficient found using the rigid lid assumption or the VoF model as the free surface boundary matched closely. However, as the blockage ratio increased to 0.5, differences in the power coefficient using the VoF model were significantly higher than obtained with the rigid lid free surface boundary.

In this study, two channels with the same mass flow rate of $132{,}850\,\frac{kg}{s}$ and different width of 21 meters and 16 meters are considered. A cross-stream array of three turbines, each 4 meters in diameter is placed at the cross section of the channel. Table 1 summarizes the flow depth and velocity for each case. The limiting flow rate and the demand for dissipating the same amount of power from the flow as the gates requires such high blockage ratios. The three methods mentioned above are used to determine the power extraction of the turbines and power dissipation from the flow.

TABLE 1- SUMMARY OF THE CASES STUDIED

Channel Width [m]	BR	Depth [m]	Velocity [m/s]
21	0.36	5	1.268
16	0.48	4.937	1.685

3 METHODOLOGY

3.1 1D Theory

In contrast to wind turbines, the HAHTs operate in open channel flows where flow is constrained by channel bed and walls along with the free surface. As flow approaches the turbine, it expands and forms a streamtube. If the area of the turbine relative to the channel cross section is significant, this streamtube is not allowed to freely expand due to the presence of channel walls and the free surface. Therefore, velocity of the flow around the streamtube increases from u_0 to u_4. The indices refer to the numbered zones in Figure 1.

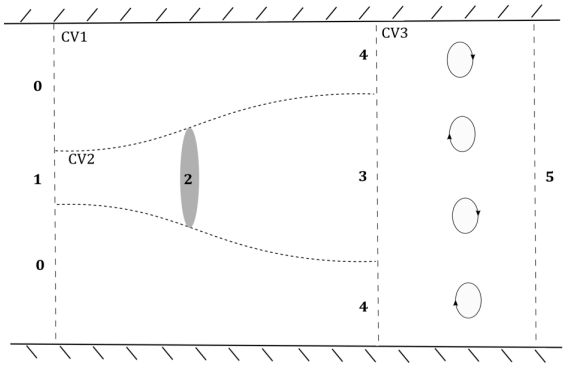

FIGURE 1.TOP VIEW OF ONE-DIMENSIONAL ACTUATOR DISC MODEL IN OPEN CHANNEL FLOW.

In this method, an actuator disc represents the turbine with the axial force that the blades exert on the flow being uniformly distributed over the rotor swept area, A_2. The slow moving wake, u_3, mixes with high velocity bypass flow, u_4, in the mixing region shown as CV3 in Figure 1.

Independent variables are upstream Froude number, $Fr_0 = \frac{u_0}{\sqrt{gh_0}}$, induction factor, $a = 1 - \frac{u_2}{u_0}$, and blockage ratio, $BR = \frac{A_2}{(A_0+A_1)}$. Conservation of mass and energy in CV1 and CV2 are used along with conservation of linear momentum in CV1 to find u_3, u_4, h_3,and $P_{turbine}$ [12]. The performance of the HAHT is characterized by the power coefficient, C_p, defined as the power extracted by the turbines, $P_{turbine}$, normalized by the kinetic power of the incoming flow as in Equation 3.1.

$$C_p = \frac{P_{turbine}}{\frac{1}{2}\rho A_2 u_0^3} = \frac{u_2}{u_0}\left[\left(\frac{u_4}{u_0}\right)^2 - \left(\frac{u_3}{u_0}\right)^2\right] \qquad 3.1$$

Where A_2 is the area of the discs. Using conservation of mass and momentum in CV3, u_5 and h_5 are found. The dissipation coefficient, $C_{dissipated}$, which determines the total power extracted from the flow relative to the incoming kinetic power is found from Equation 3.1, where $P_{dissipated}$ refers to the potential and kinetic power of the outlet subtracted from the inlet.

$$C_{dissipated} = \frac{P_{dissipated}}{\frac{1}{2}\rho A_2 {u_0}^3} \qquad 3.1$$

The following assumptions are made in the 1D theory analysis:

- By the nature of one-dimensional analysis, the power loss due to wake rotation is ignored.
- Pressure is assumed to be hydrostatic upstream of the turbine, at the end of expansion region, and at the end of the mixing region.
- Power dissipation due to drag force of the turbine blades is neglected.
- Friction losses due to channel walls are treated as negligible over the control volume.
- At the end of the expansion region and beyond, water depth is uniform across the channel.

3.2 Numerical Modeling

ADM and VBM, as developed in the commercial CFD code ANSYS Fluent 14.0, are used for this numerical modeling.

3.2.1 Reynolds-Average Navier-Stokes and $k-\omega$ SST

Open channel flows are turbulent motions that satisfy the Navier Stokes equations instantaneously. It takes large computation time and resources to capture velocity fluctuations and diffusion in turbulent flows at small scales. To reduce this requirement, Fluent solves a closed system of time-averaged equations consisting of Reynolds-Average Navier-Stokes (RANS) equations to find the flow field variables such as velocity and pressure. Conservation of mass and RANS equations of momentum conservation for an incompressible flow are presented in Equations 3.2 and 3.3.

$$\nabla . \overrightarrow{u_i} = 0 \qquad 3.2$$

$$\frac{\partial}{\partial t}(\rho u_i) + \frac{\partial}{\partial x_i}.(\rho u_i u_j) = -\frac{\partial p}{\partial x_i} + \frac{\partial}{\partial x_j}.\left[\mu\left(\frac{\partial u_i}{\partial x_j} + \frac{\partial u_j}{\partial x_i}\right) + \mu_t\left(\frac{\partial u_i}{\partial x_j} + \frac{\partial u_j}{\partial x_i}\right)\right] + \rho\overrightarrow{g_i} + S_i \qquad 3.3$$

Where u_i is the velocity vector averaged over time, ρ is the density, μ is the dynamic viscosity, μ_t is the turbulence viscosity , g_i is the gravitational acceleration, and S_i is the source/sink term. Turbulence viscosity, μ_t, is usually solved by defining different length and velocity scales using turbulence models. $k-\omega$ Shear-Stress Transport (SST) model is used in this work to close the equations. This model is a robust turbulence model and performs well in situations with adverse pressure gradients and separated flow [13].

3.2.2 Volume of Fluid Model

The volume of fluid (VOF) model is applied to the solver in order to track the free surface deflection. This model is used for multiphase flows where the position of the interface is of interest. In this technique, RANS equations are solved and the volume fraction of each phase in the fluid is tracked throughout the domain. When initiating the simulation in ANSYS Fluent, volume fraction of the region that contains water is set to 1. Once the simulation is started, surface deflects due to power extraction of the turbines to conserve mass. Volume fraction of water and air is calculated at each cell. Density and viscosity of each fluid in each cell is defined in terms of volume fraction of each phase. Volume fraction of 1 represent a cell filled with water; whereas, volume fraction of 0 means pure air. The free surface is defined where volume fraction is 0.5, based on definition in ANSYS Fluent [14].

3.2.3 Actuator Disc Model (ADM)

The turbine is modeled as a porous media that applies a constant resistance to the incoming flow over the disc area. This resistance creates a pressure drop across the porous media and reduces the velocity of the flow. Momentum in the cells of the porous media is found by adding a sink term defined by Equation 3.4 to the RANS equations.

$$S = \frac{\Delta p}{\Delta x} = -C_2 \frac{1}{2} \rho u_2^2 \qquad 3.4$$

Where Δp is the pressure drop, Δx is the thickness of the porous media, and C_2 is the inertial resistance. This constant is commonly found experimentally in the literature [8] and [7]. If experimental data is not available, Lanchester-Betz theory is used to calculate C_2 [15]. However, since this theory does not include the blockage effects, 1D theory is used to calculate this constant in this study. At a given induction factor, a, the pressure drop across the disc is found using the 1D theory discussed above. This pressure drop and u_2, calculated from the chosen induction factor, are then used to calculate C_2 from Equation 3.4.

3.2.4 Virtual Blade Model

Virtual blade modeling (VBM) uses a momentum sink term to implicitly represent the rotor. This method utilizes the blade element theory (BET) to calculate the forces applied to the blades of a turbine based on the local velocity magnitude, angle of attack, lift and drag coefficients, blade pitch angle, rotational speed of the turbine, and blade geometry. In this method, the blade is divided into sections at which the lift and drag forces are calculated using Equation 3.5.

$$dF_{L,D} = C_{L,D} \frac{1}{2} \rho c \, V^2 dr \qquad 3.5$$

Where $dF_{L,D}$ is the local incremental lift or drag forces on the blade element, $C_{L,D}$ is the lift or drag coefficients, c is the cord length, and V is the relative velocity found from Equation 3.6.

$$V = \sqrt{U^2 + (r\omega)^2} \qquad 3.6$$

In this equation, U is the local velocity at the individual cells, and ω is the rotational speed of the rotor. Normal and tangential forces are calculated based on lift and drag forces to form the sink term in the RANS equation as in Equation 3.7.

$$S_i = \frac{-\vec{F}_i}{V_{cell}} \qquad 3.7$$

Where $-\vec{F}_i$ is the force vector that each blade element exerts on the flow over one revolution and V_{cell} is the volume of each cell. In this model, the tip effect is set to 96%, which means only 96% of blade span's lift force is taken into account and the remaining (tip region) is set to 0. However, drag force is assumed to be present along the entire blade.

3.2.5 Domain geometry and mesh

The computational domain is created based on the geometry of a constructed irrigation canal in the West Canal of the Columbia Basin Project where the flow rate is known. The channel cross-section is a trapezoid. However, a rectangular channel of equivalent area is assumed here, of 21m width; and a constricted case is also considered where channel width is lowered to 16m while keeping flow rate constant. Blockage ratio is 0.36 and 0.48 for the wide and narrow channels, respectively; while Froude number is 0.18 and 0.24. Three turbines, each 4m in diameter, are placed 1m apart from one another across the channel and 2.5m above the channels' bottom wall as shown in Figure 2.

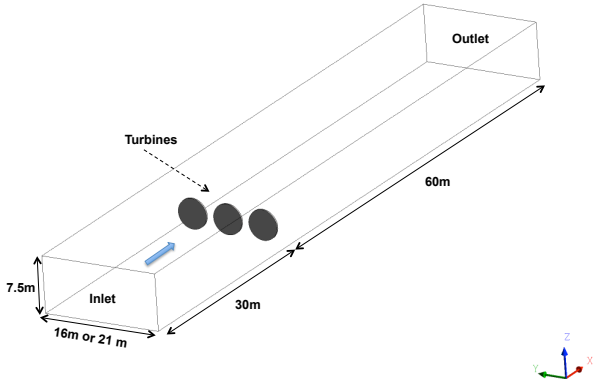

FIGURE 2. GEOMETRY OF THE COMPUTATIONAL DOMAIN

This domain is spatially discretized to small hexahedral control volumes. An unstructured quad (pave) mesh is created on the cross-sectional area where turbines are placed. This mesh is then extruded to create the 3D mesh of the channel in GAMBIT.

This grid must be refined near the free surface in order to capture free surface deflections that occur due to power extraction by the turbines and avoid numerical instabilities that may be caused due to density variation at the free surface. Therefore, once a stable and converged solution is found, the mesh is refined where the volume fraction varies between 0.4 and 0.6. This procedure is continued until the solution is independent of the mesh resolution. The final mesh consists of 3.3 million hexahedral cells for the 16m wide channel and 4.2 million cells for the 21m wide channel. Orthogonal quality is 0.8 for

both channels' mesh, which indicates that the domains are well discretized [14].

3.2.6 Boundary Condition

The inlet boundary condition of all simulations is the mass flow rate at inlet and this is kept at 132,850 kg/s for water and 50 kg/s for air. The free surface level at inlet and outlet is 5m and 4.937m for the wide and narrow channel respectively. Fluent treats the free surface level at the inlet as an initial condition while keeping the outlet free surface as a boundary condition. Therefore, free surface at the inlet is adjusted throughout the simulation to conserve mass as velocity changed throughout the domain due to the effects of the turbines. The outlet boundary condition is set as a pressure outlet.

Turbulence at the inlet and outlet is defined by introducing turbulence intensity, I, and hydraulic diameter, D_H. Turbulent intensity is usually determined from experiments to feed into the CFD for inlet boundary conditions. However, since no turbulence measurement is taken at the channel, a low turbulent intensity of 1% is picked for the inlet. As mentioned in Introduction, higher values of ambient turbulence intensity result in faster wake recovery. By choosing the low turbulence intensity level at the inlet, results from the simulations represent the slowest wake recovery expected. It is assumed that far downstream of the turbines, the flow recovers to the original state; therefore, turbulence intensity is set to 1% at the outlet. Boundary conditions used in the simulation are summarized in Table 2.

TABLE 2. BOUNDARY CONDITION USED IN ADM FOR 21M AND 16M WIDE CHANNELS RESPECTIVELY.

Mass Flow inlet	Water: 132,850 [kg/s] Air: 50 [kg/s] Free Surface Level: 5m, 4.937m I: 1% D_H: 8m, 7.545m
Pressure Outlet	Free surface Level: 5m, 4.937m I: 1% D_H: 8m, 7.545m
Channel bed and walls	No slip
Top wall	Symmetry

3.2.7 Blade Design

For the case of a HAHT, it is desirable to have a high lift to drag ratio along the blade in order to maintain a high efficiency, while delaying cavitation inception as much as possible [16]. The NACA 63-815 airfoil has been shown to perform well for marine turbines; thus, it has been used in this work [17], [18], [19]. The experimental lift and drag coefficients with respect to the angle of attack are presented in Figure 3 [18].

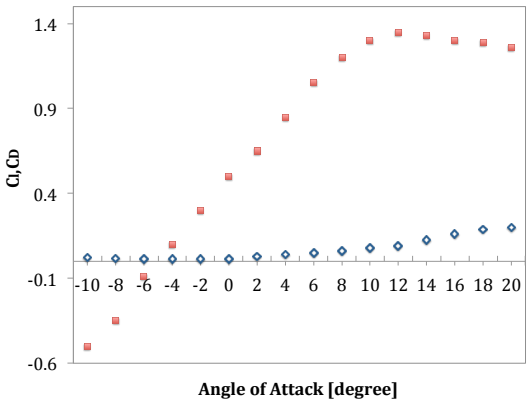

FIGURE 3. LIFT COEFFICIENT VERSUS ANGLE OF ATTACK FOR NACA 63-815 AIRFOIL [18].

VBM is utilized to design and optimize the blades' geometry since the flow field along the blades is highly influenced by the blockage in the case of BR=0.48. BET calculation is used to find local pitch angles along the blade (i.e. the local twist angle, $(\boldsymbol{\theta})$, in Table 3) that produce maximum possible power; then VBM is used in an iterative manner to find the chord distribution that optimizes the power. Blade geometry is provided in Table 3. In this table, R is the radius of the turbine and r is the local radius from the center of the turbine.

TABLE 3. BLADE GEOMETRY

$\frac{r}{R}$	$\frac{c}{R}$	Twist (θ)
0.2	0.250	27.0
0.3	0.240	19.0
0.4	0.235	11.1
0.5	0.230	8.9
0.6	0.225	7.0
0.7	0.220	6.0
0.8	0.210	3.0
0.9	0.205	1.0
1.0	0.205	0.6

Considering that the turbines operate in channels with high blockage ratios, where the free surface is near the turbine blades, it is important to perform cavitation analysis to understand the limits of turbine operating conditions (i.e. TSR and the pitch). Cavitation is the formation of vapor bubbles within a flowing fluid, and occurs when

the pressure of the fluid falls below the vapor pressure. Cavitation decreases the lift force acting on the airfoil, increases the drag force, and can damage the blades. The onset of cavitation is found to occur when the minimum negative pressure coefficient, $-C_{pres}$, is equal to or higher than the cavitation number, σ [20].

$$\sigma = \frac{P_{atm} + \rho g h - P_v}{\frac{1}{2}\rho V^2} \qquad 3.8$$

In this equation, P_{atm} is the atmospheric pressure, h is the depth of emersion, V is the relative velocity, and P_v is the vapor pressure. At the tip of the blade, depth of emersion is lowest and local relative velocity is the highest. Therefore, cavitation number is lowest and it is reasonable to assume that should cavitation occur at a particular TSR, it will occur near the tip. Figure 4 shows the cavitation number calculated at the tip versus angle of attack, α and compares these values to $-C_{pres}$. At a TSR of 6, cavitation numbers at different angles of attack are close to the $-C_{pres}$ and cavitation is expected for $\alpha > 6$ degrees. Thus is it desirable to operate the turbines at TSR<6. In order to further investigate the operating condition, pitch angle is varied at the tip from -10 to 10 at TSR=5. Cavitation is not expected in this operating region as long as $\alpha < 10$.

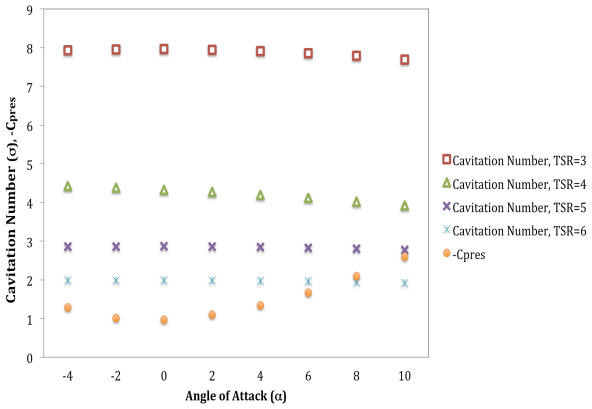

FIGURE 4. CAVITATION NUMBER AND MINIMUM NEGATIVE PRESSURE COEFFICIENT VERSUS ANGLE OF ATTACK (AT $\theta_{p,0} = 0$).

4 RESULTS

4.1 1D Theory

In this section, 1D theory is used to understand the effects of blockage ratio on free surface elevation and useful power extraction of an array of three turbines placed side by side across the channel. Blockage ratio is increased from 0.36 to 0.48 while Froude number varies from 0.18 to 0.24. As the blockage ratio reaches 0.48, two different solutions are found. One responds to a subcritical solution shown by the solid red line in Figure 5 and the other one is the supercritical solution shown by the red dashed line. As the channel becomes more constricted, surface drop increases behind the turbines at all induction factors. In the supercritical case, the bypass flow accelerates strongly, causing the free surface to drop dramatically, such that a hydraulic jump (not shown) may occur downstream of the turbines.

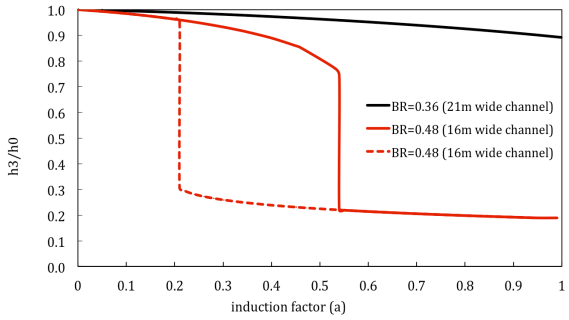

FIGURE 5. EFFECT OF CHANNEL CONSTRICTION ON SURFACE DROP AT THE END OF THE EXPANSION REGION.

The presence of a free surface and channel walls creates a high blockage ratio for HAHTs operating in constructed channels. Figure 6 shows a wide range in power coefficients (i.e. power extraction efficiencies) for HAHTs operating at high blockage ratio. If one focuses on the subcritical cases (i.e. the solid blue and black lines, and the solid red line to the left of the jump to supercritical flow), peak power coefficients vary from about 1.6 (160%) for the 21 m wide channel to about 4.0 (400%) for the 16 m wide channel.

These high efficiencies are caused by the blockage effect and the conversion of both kinetic and potential energy to the energy of the turbine. The Lanchester-Betz theory considers only the conversion of kinetic power to turbine power. For the supercritical regime even greater efficiencies are indicated.

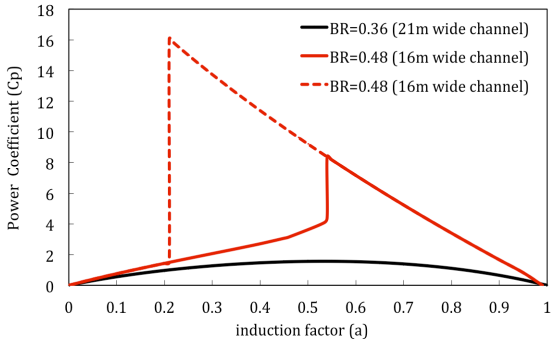

FIGURE 6. EFFECT OF CHANNEL CONSTRICTION ON POWER PRODUCTION

4.2 ADM

As discussed in the previous section, blockage effects of the channel walls and bed along with the free surface increase as higher blockage is introduced in the channel. Figure 7 a) and b) show the increase in velocity of the bypass flow as it passes around the actuator discs for BR=0.48 and BR=0.36 cases. Higher bypass velocity is achieved as blockage ratio is increased. Since ADM applies a constant resistance to the flow, a uniform velocity is observed close behind the turbines.

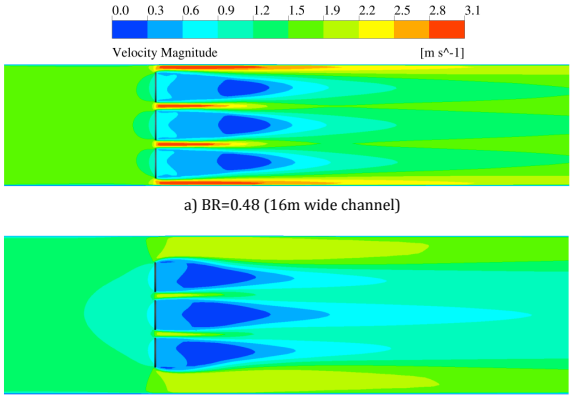

a) BR=0.48 (16m wide channel)

b) BR=0.36 (21m wide channel)

FIGURE 7. TOP VIEW OF VELOCITY MAGNITUDE PLOTS ON A PLANE PARALLEL TO THE CHANNEL BED PASSING THROUGH THE CENTER OF DISCS. A) 16M WIDE CHANNEL, BR=0.36, FR=0.18 B) 21M WIDE CHANNEL (SUBCRITICAL), BR=0.48, FR=0.24

Figure 7 shows that flow is locally induced (i.e. reduce) close upstream of each turbine for both cases. However, the lower blockage case presents an array induced velocity in addition to the velocity induction at individual turbines. This is further investigated in Figure 8 by plotting normalized velocity magnitude at the centerline of the turbines along the cross-section of the channel 1 diameter upstream of the turbines for the cases of BR=0.36 and BR=0.48. At high blockage ratio of 0.48, the flow needs to accelerate dramatically to conserve mass as it passes around the turbines; therefore, flow upstream of the turbines does not see the effects of the array.

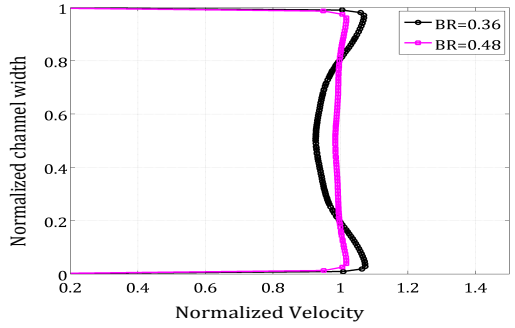

FIGURE 8. NORMALIZED VELOCITY VERSUS THE NORMALIZED CHANNEL WIDTH 1D UPSTREAM OF THE TURBINES.

In order to investigate the wake recovery, velocity magnitude is normalized by upstream velocity and plotted against normalized depth (by upstream depth) 5 diameters (5D) upstream, 5D, 10D, and 15D downstream of the middle turbine for each channel in Figure 9. The overall wake recovery is faster as blockage ratio is increased. Velocity magnitude almost reaches the free stream velocity 15D downstream of the turbines at BR=0.48.

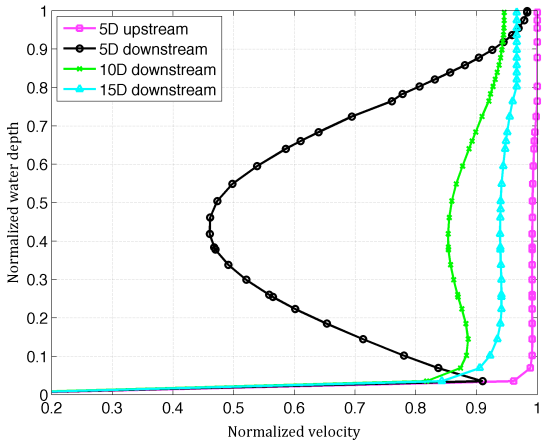

a) BR=0.48 (16m wide channel)

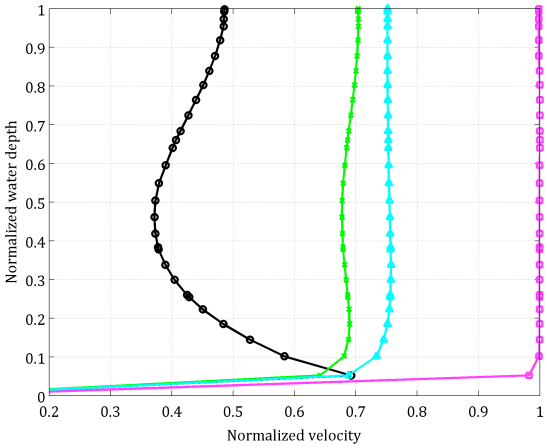

b) BR=0.36 (21m wide channel)

FIGURE 9. NORMALIZED DEPTH VERSUS NORMALIZED VELOCITY 5D UPSTREAM, 5D, 10D AND 15D DOWNSTREAM OF THE MIDDLE TURBINE FOR A) BR=0.48 (16M WIDE CHANNEL) AND B) BR=0.36 (21M WIDE CHANNEL). THE TURBINE AXIS IS LOCATED AT NORMALIZED DEPTH OF 0.5.

Dynamic pressure plots of the vertical plane passing through the center of the middle turbine are presented in Figure 10. Dynamic pressure, q, is the kinetic energy per unit volume of the fluid and is defined as

$$q = \frac{1}{2}\rho u^2 \qquad 4.1$$

When dealing with open channel flows, it is difficult to distinguish velocities of each phase. By using dynamic pressure, it is possible to visualize

how fast each fluid moves, since velocity is squared in its definition, and to distinguish the free surface, due to dependency on density.

Tracking the free surface using the VOF model is important in predicting the power extraction of turbines in high blockage ratios. The ADM is used to investigate the effect of disregarding the free surface deflections on performance prediction of the turbines. The VoF model is turned off in ANSYS Fluent 14.0 and the region corresponding to air is subtracted from the grid to maintain the desired blockage ratio. The top boundary condition is set to free slip condition (rigid lid). The results show that power extraction by turbines is underpredicted when the free surface is not included in the simulation. The underprediction of power coefficient increases as blockage ratio is raised (i.e. power is underpredicted by 12% when BR=0.48 and 7% when BR=0.36). Therefore, it is important to use the VoF model to track the surface.

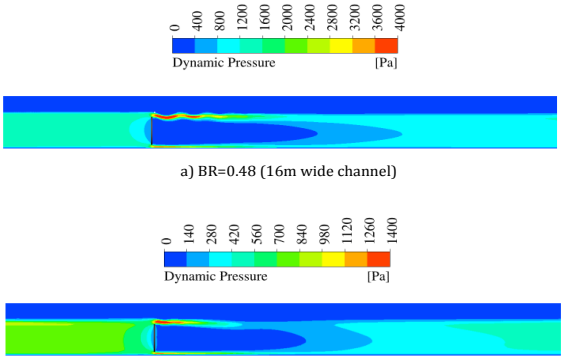

FIGURE 10. DYNAMIC PRESSURE PLOT OF A VERTICAL PLANE PASSING THROUGH THE CENTER OF MIDDLE TURBINE.

4.3 VBM

1D theory and ADM were used in the previous sections to understand the blockage effects on the surface drop and power extraction of the turbines at two different BRs. In this section, the VBM is used only for the case with BR=0.48. Figure 11 shows the top view of the velocity field on a plane passing through the center of the turbines at the designed condition (TSR=5 and $\theta_{p,0} = 0$).

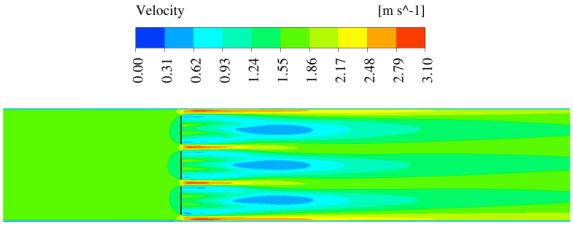

FIGURE 11. TOP VIEW VELOCITY CONTOUR PLOT OF THE OPTIMIZED TURBINE DESIGN (TSR=5 AND $\theta_{p,0} = 0$) AT THE PLANE PASSING THROUGH THE CENTER OF TURBINE.

Normalized depth is plotted in Figure 12 versus normalized velocity at 5D upstream, and at 5D, 10D, and 15D downstream of the middle turbine in the 16m wide channel using the VBM. VBM compared to ADM gives some differences near the channel bed. For 5D downstream, VBM appears to show a more pronounced velocity magnitude in this region than ADM, with the peak normalized velocity reaching 1.17 versus about 0.90 with ADM. Also, with VBM, the wake recovery is somewhat slower than with ADM.

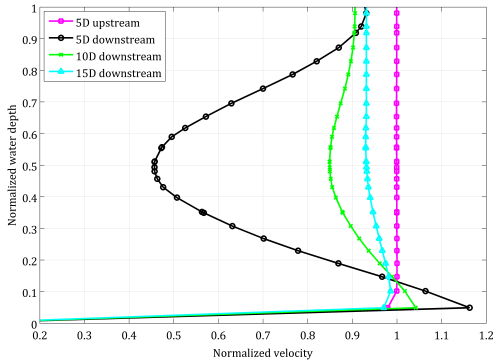

FIGURE 12. NORMALIZED DEPTH VS NORMALIZED DEPTH 5D UPSTREAM, 5D, 10D, AND 15D DOWNSTREAM OF THE TURBINES IN THE 16M WIDE CHANNEL (BR=0.48).

Power coefficient versus pitch angle is plotted in Figure 13 for cases with the TSR=5 and TSR=3.5. At both TSRs, power coefficients exceed the Lanchester-Betz limit due to the confining effects of the channel and the free surface. Power coefficient is sometimes higher than 1, since HAHT placed in high blockage flows extracts potential energy of the flow in addition to its kinetic energy.

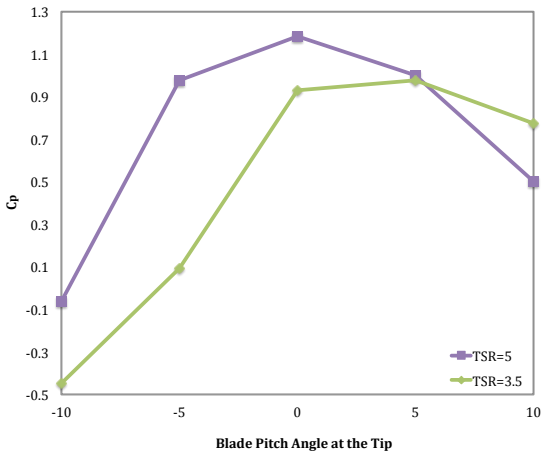

FIGURE 13. POWER COEFFICIENT AT TSR=5 AND 3.5 VERSUS PITCH ANGLE FOR BR=0.48 (16M WIDE CHANNEL).

Dissipation Coefficient, $C_{dissipated}$ is calculated for cases mentioned above and is plotted in Figure 14. This power dissipation is due to all losses in

the kinetic and potential power of the water between the inlet and outlet of the domain treated. Its value is highest when some sections of the blades stall while other sections produce good lift. The power dissipated at the design condition, TSR=5 and $\theta_{p,0} = 0$, is 270 kW which suggests the need for 4 arrays of turbines placed at least 15D apart from one another to dissipate as much power as a row of gates placed across the channel (about 1MW). The useful power extracted by the turbines is about 93kW per 3-turbine array.

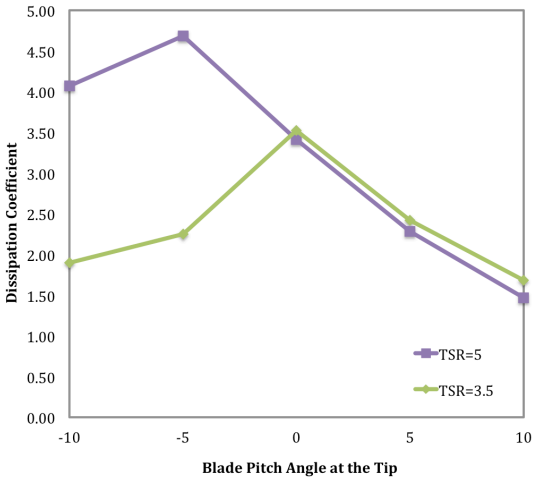

FIGURE 14. TOTAL POWER DISSIPATION EFFICIENCY VERSUS BLADE PITCH AT THE TIP FOR TSR OF 3.5 AND 5 FOR THE 16M WIDE.

4.4 Comparison Between Models

In order to compare VBM to ADM and one-dimensional theory, the VBM is used to calculate parameters such as induction factor and thrust coefficient of the turbines at desired TSR and $\theta_{p,0}$ at BR=0.48. Thrust coefficient, C_t, is then found using Equation 4.2.

$$c_t = \frac{Thrust}{\frac{1}{2}\rho A_2 {u_0}^2} \qquad 4.2$$

The only parameters needed by the one-dimensional theory are BR, Fr, and induction factor to calculate useful power extraction by turbines and power dissipation from the flow to compare to the VBM results. ADM uses the induction factor along with the thrust coefficient found using VBM to calculate the pressure drop across the actuator discs and consequently the inertial resistance, C_2 from Equation 3.4.

Table 4 provides calculated induction factor and Thrust using VBM for the turbines operating at designed condition of TSR=5 and $\theta_{p,0} = 0$. Induction factor and thrust coefficient are then used in ADM and one-dimensional theory to provide a direct comparison between these models to VBM. The difference in induction factor using the ADM is due to the fact that ANSYS Fluent allows the surface elevation to increase at the inlet (consequently the inlet velocity to increase) from the defined inlet boundary conditions (while keeping mass flow rate constant), as mentioned in Section 3.2.6.

TABLE 4- SUMMARY OF SOME RESULTS FROM COMPARING THE MODELS AT INDUCTION FACTOR OF 0.243 AND THRUST OF 45.8 KN.

	a	$h_0\ [m]$	$u_0\ \left[\frac{m}{s}\right]$	$Thrust\ [kN]$
VBM	0.243	5.15	1.62	45.8
ADM	0.289	5.11	1.63	39.5
1D theory	0.243	4.937	1.69	40.33

One-dimensional theory and ADM overpredicted the extracted power from the turbines by about 43 percent compared to the VBM as shown in Figure 15. Both one-dimensional theory and ADM use the pressure drop across the turbine to find power extracted by turbines, whereas, power is calculated by the time-average torque multiplied by the rotational speed of the turbines in VBM. The VBM is considered to provide a more realistic power extraction by turbines since it takes into account the geometry of the blades, hub of the turbine, tip effects, and drag.

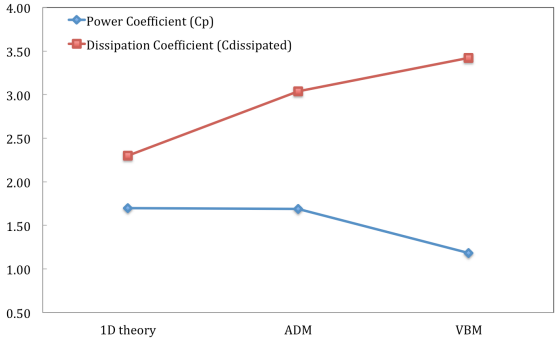

FIGURE 15. COMPARISON BETWEEN ONE-DIMENSIONAL THEORY, ADM AND VBM FOR POWER COEFFICIENT AND DISSIPATION COEFFICIENT AT TSR=5, $\theta_{p,0} = 0$, AND INDUCTION FACTOR OF 0.24.

The total power dissipated from the flow is underpredicted using the one-dimensional theory and ADM compared to VBM by 30 and 10 percent respectively. Power dissipation using one-dimensional theory and ADM is due to useful power extracted by the turbines and power dissipation of the mixing region. The power dissipated calculated using VBM includes the losses due to useful power extraction of turbines, mixing of wake with bypass flow, drag forces of

the turbine, mixing of the rotational flow field generated based on geometry of the turbines in addition to the wake rotation.

Computation time varied from 2 days to 6 hours for VBM and ADM respectively using 12 processors. On the other hand, any result is found instantly using 1D theory.

5 CONCLUSION

Traditionally, gates are used to control water flow in waterways by dissipating energy of the flow. Horizontal axis hydrokinetic turbines (HAHT) are good candidates to replace these traditional gates to extract power from the flow in terms of useful power and control the flow.

5.1 Summary of models

Theoretical and numerical approaches are used to model HAHTs in open channel flows. The theoretical method uses one-dimensional control volume analysis to predict maximum power that an ideal rotor can extract from the flow as useful power and as wake mixing loss at a given Froude number and blockage ratio. This method is then compared to the three-dimensional actuator disc model (ADM) developed in the commercial computational fluid dynamic (CFD) code ANSYS Fluent. This model uses a porous media to represent the HAHTs and Reynolds-Average Navier-Stokes (RANS) equations along with the volume of fluid (VoF) model to solve for the flow field and track the free surface. Then the same computational modeling is implemented with a more advanced model, the virtual blade model (VBM), which uses blade element theory (BET) to consider geometry of the blades and operating conditions such as the tip speed ratio (TSR) and blade pitch angle. This method is used to optimize the turbine geometry for maximum power and to find operating limits to avoid blade cavitation.

5.2 Summary of the blockage effects on the extracted power by turbines

The presence of a free surface and channel walls creates a high blockage ratio for HAHTs. It is found that turbines extract more power as blockage ratio increases. At a mass flow rate of 132,850 $\frac{kg}{s}$, a cross-stream array of three turbines, each 4 meters in diameter, produces 3 times more power when the blockage ratio is 0.48 (and Froude number is 0.24) compared to the case when the blockage ratio is 0.36 (and Froude number is 0.18). In this case, extraction efficiency, C_p is 1.5 times higher for the case with higher blockage using 1D theory and ADM.

Tracking the free surface using the VOF model is important in predicting power extraction of turbines in high blockage ratios. Power extraction by turbines is underpredicted when the free surface is not included in the simulation (by using a lid as the top boundary condition in the computational domain, while maintaining the desired blockage ratio). Using ADM, the underprediction of power extraction increases, as blockage ratio is raised (i.e. power is underpredicted by 12% when BR=0.48 and 7% when BR=0.36).

ADM shows that flow is only locally induced at the turbines for high blockage ratios (i.e. BR=0.48). The lower blockage case (i.e. BR=0.36) shows an array induced velocity in addition to the velocity induction by individual turbines. An array wake is also observed for the lower blockage case.

It is important to study the wake of HAHTs in order to investigate the placement of arrays of turbines in the channel. Wake recovery is faster for the flow when the blockage ratio is high compared to the flow at a lower blockage. This tendency appears to be caused by the higher velocity through and around the turbines when blockage ratio is high. This enhances the mixing of fast and slow moving flows behind the turbine in near and far wake regions.

5.3 Summary of the blockage effects on the free surface deflection and the total dissipated power from the flow

Turbines extract more power in a channel with higher blockage ratio. Consequently, a higher free surface drop behind the turbines occurs for the flow in a higher blockage ratio case compare to a lower blockage ratio flow. The flow depth far downstream of the turbines normalized by upstream depth is lower for the higher blockage case (BR=0.48) compared to the lower blockage ratio (BR=0.36) as shown by the 1D theory and ADM.

Total power dissipated from the flow in the one-dimensional and ADM treatments is due to the power extraction of the flow by turbines and mixing of the slow moving flow behind the turbine and fast moving water around the turbines. Higher total power is dissipated from the flow at higher blockage ratios. This is due to higher power extraction by the turbines and higher shear between the fast and slow moving water behind the turbines at the higher blockage ratios compared to lower blockage ratios.

5.4 Summary of comparison between three models

The VBM is used to calculate parameters such as induction factor and thrust coefficient of the turbines at the desired TSR and blade pitch. These parameters are used to compare power extraction and power dissipation coefficients using the one-dimensional theory and ADM to VBM results.

The one-dimensional theory and ADM overpredict the extracted power compared to the VBM. Both one-dimensional theory and ADM use the pressure drop across the turbine to find power extracted by turbines, whereas, power is calculated by the torque multiplied by the rotational speed of the turbines in VBM. The simplification used in calculations of power using one-dimensional and ADM results in about 43% overprediction of power extracted by the turbines.

The total power dissipated from the flow is underpredicted using the one-dimensional theory and ADM compared to VBM by 30 and 10 percent respectively.

5.5 Future work

The literature lacks the experimental data for power extraction of HAHTs in high blockage ratio flows. Experiments must be performed using the designed turbine to validate the three-dimensional numerical and one-dimensional theoretical results. A new set of boundary condition must be developed in Fluent so that the inlet water depth can be fixed. This ensures the correct inlet velocity and consequently the correct velocity at the turbines.

6 ACKNOWLEDGEMENTS

This paper is based on the MSME Thesis of Ms. Hosenyi-Chime. The authors would like to thank the Department of Energy for the support of this work. The authors also wish to thank Drs Novosselov and Karalus for their valuable assistance.

7 REFERENCES

[1] Corten G. P., 2000, "Heat Generation by a Wind Turbine," 14th IEA Symposium on the Aerodynamics of Wind Turbines, pp. 1–8.

[2] Garrett C., and Cummins P., 2007, "The efficiency of a turbine in a tidal channel," Journal of Fluid Mechanics, **588**, pp. 243–251.

[3] Whelan J. I., Graham J. M. R., and Peiró J., 2009, "A free-surface and blockage correction for tidal turbines," Journal of Fluid Mechanics, **624**(March 2009), p. 281.

[4] Polagye B., 2009, "Hydrodynamic Effects of Kinetic Power Extraction by In-Stream Tidal Turbines," University of Washington.

[5] Macleod A. J., 2002, "Wake effects in tidal current turbine farms," Proceedings of MAREC Conference, Newcastle.

[6] Sun X., Chick J. P., and Bryden I. G., 2008, "Laboratory-scale simulation of energy extraction from tidal currents," Renewable Energy, **33**(6), pp. 1267–1274.

[7] Sun X., 2008, "Numerical and Experimental Investigation of Tidal Current Energy Extraction," University of Edinburgh.

[8] Harrison M. E., Batten W. M. J., Myers L. E., and Bahaj A. S., 2009, "A comparison between CFD simulations and experiments for predicting the far wake of horizontal axis tidal turbines," Proceedings of the 8th European Wave and Tidal Energy Conference, Uppsala, Sweden, pp. 566–575.

[9] Nishino T., and Willden R. H. J., 2012, "Effects of 3-D channel blockage and turbulent wake mixing on the limit of power extraction by tidal turbines," International Journal of Heat and Fluid Flow, **37**, pp. 123–135.

[10] Batten W. M. J., Harrison M. E., and Bahaj a S., 2013, "Accuracy of the actuator disc-RANS approach for predicting the performance and wake of tidal turbines.," Philosophical transactions. Series A, Mathematical, physical, and engineering sciences, **371**(1985), p. 20120293.

[11] Consul C. A., Willden R. H. J., Mcintosh S. C., and A P. T. R. S., 2013, "Blockage effects on the hydrodynamic performance of a marine cross-flow turbine," Philosophical transactions. Series A, Mathematical, physical, and engineering

sciencesransactions of the Royal Society, (January).

[12] Hoseyni Chime A., 2013, "Analysis of Hydrokinetic Turbines in Open Channel Flows," University of Washington.

[13] Menter F. R., 1996, "A comparison of some recent eddy viscosity turbulence models," Journal of Fluids Engineering, **118**, p. 514.

[14] "Ansys Fluent 14.0 User's Guide, Chapter 29, Modeling Using the Solver, 2011."

[15] Teymour A., and Mozafari J., 2010, "Numerical Modeling of Tidal Turbines : Methodology Development and Potential Physical Environmental Effects," University of Washington.

[16] Manwell, J.F, McGowan, J.G, Rogers A. ., 2006, Wind Energy Explained, Wiley, Amherst, USA.

[17] Batten W. M. J., Bahaj a. S., Molland a. F., and Chaplin J. R., 2007, "Experimentally validated numerical method for the hydrodynamic design of horizontal axis tidal turbines," Ocean Engineering, **34**(7), pp. 1013–1020.

[18] Molland a F., Bahaj a S., Chaplin J. R., and Batten W. M. J., 2004, "Measurements and predictions of forces, pressures and cavitation on 2-D sections suitable for marine current turbines," Proceedings of the Institution of Mechanical Engineers, Part M: Journal of Engineering for the Maritime Environment, **218**(2), pp. 127–138.

[19] Batten W. M. J., Bahaj a. S., Molland a. F., and Chaplin J. R., 2008, "The prediction of the hydrodynamic performance of marine current turbines," Renewable Energy, **33**(5), pp. 1085–1096.

[20] Batten W. M. J., Bahaj a. S., Molland a. F., and Chaplin J. R., 2006, "Hydrodynamics of marine current turbines," Renewable Energy, **31**(2), pp. 249–256.